Development of High-Current Superconducting Accelerators at Argonne National Laboratory

J. R. Delayen, C.L. Bohn, W.L. Kennedy, B.J. Micklich, C.T. Roche, and L. Sagalovsky
Argonne National Laboratory, Engineering Physics Division
9700 South Cass Avenue, Argonne, Illinois 60439

Abstract

Superconducting linacs may be a viable option for high-current applications such as fusion materials irradiation testing, spallation neutron source, transmutation of radioactive waste, tritium production, and energy production. These linacs must run reliably for many years and allow easy routine maintenance. Superconducting cavities operate efficiently with high cw gradients, properties which help to reduce operating and capital costs, respectively. However, cost-effectiveness is not the sole consideration in these applications. For example, beam impingement must be essentially eliminated to prevent unsafe radioactivation of the accelerating structures, and thus large apertures are needed through which to pass the beam. Because of their high efficiency, superconducting cavities can be designed with very large bore apertures, thereby reducing the effect of beam impingement. Key aspects of high-current cw superconducting linac designs are explored in this context.

I. INTRODUCTION

Questions regarding the design of linear accelerators with high duty factor for the long-term production of high-current ion beams center as much on beam physics as on hardware. The pervasive concern is whether dynamical phenomena which generate a diffuse halo of beam particles can be sufficiently controlled to limit radioactivation induced by beam impingement to safe levels. For example, as indicated in Section II below, the maximum tolerable amount of beam impingement is of the order of 0.03 nA/m for 1 GeV protons. The heat load associated with this level of impingement is 30 mW/m. The rf losses on a superconducting cavity will be ~20-40 W/m, and therefore radioactivation is by far the dominant concern related to beam impingement on superconducting structures. This concern is equally important for copper accelerators. Because shunt impedance is of less concern in superconducting cavities, they can be designed to operate at low frequency and with large bore-hole apertures to mitigate impingement. These constitute additional degrees of freedom which are available in the design of high-current linacs. In Section III below, we provide four generic superconducting cavity geometries designed specifically for use in these high-current linacs, and we present design considerations for superconducting RFQs as well as other relevant developments in beam physics. In Section IV we highlight recent progress toward a conceptual understanding of beam-halo formation and emittance growth, and the development of a corresponding semianalytic dynamical formalism.

II. LIMITS ON PERMISSIBLE RADIOACTIVATION

For a low-energy (40 MeV) deuteron accelerator, such as that being proposed for a d+Li neutron source for fusion materials testing, the most important reactions are the (d,p) and (d,2n) reactions, with (d,n), (d,α), and other reactions being somewhat less important. The neutrons produced through (d,xn) reactions can also produce activation. Experiments have shown that neutron yield is higher in copper than in niobium by a factor of about two[1] at E_d=10-15 MeV, and we use that assumption up through 40 MeV. This is consistent with the variations in (n,2n) cross sections such as shown by Barbier.[1]

Radionuclides produced from niobium have either very short or very long half-lives. Thus, the dose rate beginning a few hours after shutdown should be smaller relative to that from copper. For niobium, the dominant dose from direct D activation is due to $^{93}Mo^{m}$ (6.9 h). The neutron-induced activity in niobium is predominantly due to $^{92}Nb^{m}$ (10.13 d) .

For copper, ^{63}Zn (38.3 m) and ^{62}Cu (9.8 m) dominate the dose rate at short times following irradiation. Of particular interest is ^{65}Zn (243.8 days), since this nuclide builds up over long irradiations and thus dominates the dose rate after several days for irradiation times of around 300 days. Other (d,p) and (d,2n) activities in Cu decay rapidly. At longer times following shutdown, ^{64}Cu (12.8 h) can also be important, as well as ^{60}Co (5.27 y) from $^{63}Cu(n,\alpha)$ for long irradiation times.

Accelerator activation was estimated for a constant 1 nA/m current loss and an average gradient of 1 MV/m, with the results shown in Table 1. For 30 days irradiation time (t_{irr}), the copper dose is much higher for short time after shutdown (t_{sh}). The dose for niobium is higher from a few hours to a few days following shutdown (due to $^{92}Nb^{m}$), while the copper is again higher at 30 days, although the difference is small. For an irradiation time of 300 days, the dose in copper is higher at all times following shutdown because of the ingrowth of ^{65}Zn. Dose rates are relatively insensitive to gradient, decreasing somewhat at higher gradient, assuming a constant deuteron loss per unit length. However, the amount of irradiated material will be greater for a lower gradient (longer accelerator).

Table 1. Dose rates in mrem/h at 30 cm distance from copper and niobium 35-MeV D accelerators for 1 nA/m current loss and 1-to-5 MV/m average gradient.

t_{sh}	Cu	Nb	Cu	Nb
	t_{irr} = 30 days		t_{irr} = 300 days	
0 h	21.	4.4	23.	4.4
1 h	5.7	4.2	7.4	4.2
8 h	2.0	3.1	3.8	3.1
24 h	1.0	2.2	2.7	2.2
30 d	0.43	0.31	2.1	0.31

For high-energy proton accelerators, neutron yields increase with higher Z for proton bombardment. The range of 1 GeV protons in both niobium and copper is of order 40 cm,[2] and because the wall thickness of the cavities is much less than the range, radioactivation of niobium should be slightly more, but comparable to, that of copper. Thus, for a proton beam, the current loss in both niobium and copper needs to be less than 0.2 nA/m at 200 MeV, and less than 0.03 nA/m at 1 GeV, to be under 2.5 mrem/hr at a distance of 1 m from the linac one hour after shutdown.[3]

III. SUPERCONDUCTING STRUCTURES

1. General considerations

Geometries of low-velocity superconducting resonators generally incorporate an inner conductor which provides a TEM-like accelerating mode.[4] The center-gap to center-gap distance in these structures is of order $\beta\lambda/2$, where $\beta = v/c$ is the beam velocity, and λ is the rf wavelength. For velocities less than $\sim 0.1c$ and frequencies of several hundred MHz, this distance becomes too small for practical resonators,

and this consideration is a principal motivator for superconducting RFQs which provide proton energies to ~8 MeV.[5] For proton energies ranging from 8 MeV to 2 GeV, the corresponding velocity range is ß=0.1-0.9. Superconducting resonators have recently been developed for frequencies in the range 350-850 MHz and optimized for velocities up to ß=0.3. Off-line experiments with these structures have yielded high accelerating gradients.[6,7] Of these structures, the easiest to fabricate is the spoke resonator shown in Fig. 1. This geometry is also modular, for several units can be stacked together to make a multigap cavity. For these reasons, we use the spoke as the baseline geometry for superconducting cavities to be used in high-current linacs.

The choice of frequency hinges on a number of considerations. One of them is the ability to provide large-bore apertures for the beam, and this favors lower frequencies and larger cavities. Large bores also provide lower transverse shunt impedances which reduce cumulative beam break-up. The availability of rf power is a second concern.

On the other hand, it has been inferred from numerical simulations that high frequencies mitigate emittance growth by lowering the charge per bunch.[8] This is a major consideration when emittance preservation is crucial. For most of the high-current applications, however, emittance growth is a concern only in connection with halo formation and beam transport. A detailed understanding of the effects of bunching on high-current beams is a fundamental building block for the design of these linacs, and this will be the topic of future investigations.

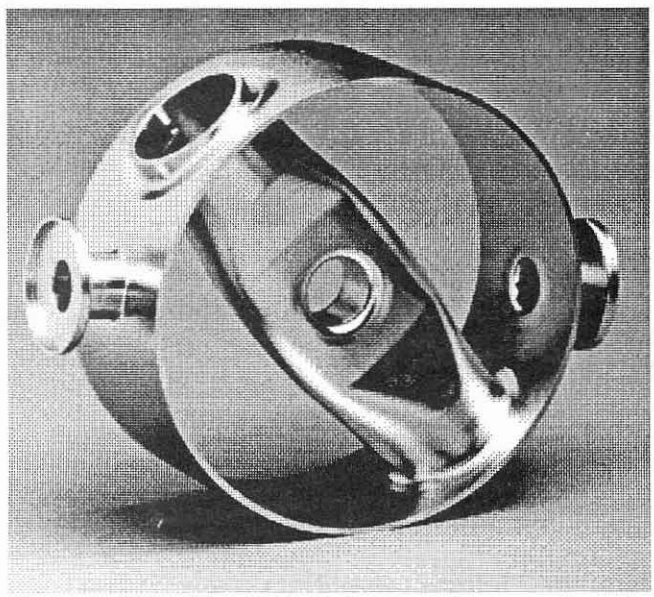

Figure 1. 850 MHz, β=0.28, 2-gap spoke resonator prior to the welding of the end plates.

One possible strategy for achieving high currents is to combine two beams by funneling them together at a relatively low energy, a process which doubles the rf frequency. To achieve large bores and use a common frequency for rf power amplifiers, we shall assume the linac operates at 350 MHz, and that prior to funneling, the frequency is 175 MHz.

2. *Large-bore superconducting cavity geometries*

As shown in the examples of Figs. 2 and 3, the spoke geometry can be adapted to span a wide velocity range. For high velocities it becomes more practical to introduce single-cell structures like that shown in Fig. 4, or multicell structures like that shown in Fig. 5. The properties of these large-bore geometries, which were calculated with MAFIA in the case of the spoke resonators and SUPERFISH in the case of the "elliptical" cavities, are given in Table 2 below. In the Table, resonators #1-#4 refer to the 175 MHz, ß=0.125 spoke, the 350 MHz, ß=0.45 spoke, the 350 MHz, ß=0.45 single-cell, and the 350 MHz, ß=0.8 two-cell, respectively.

Compared to two-gap spoke resonators, two-cell "elliptical" cavities generally have higher shunt impedances and lower rf surface fields. They are also comparatively simple and easy to fabricate. However, for a given frequency, these structures are also much larger than the spoke, and are likely to be less mechanically rigid.

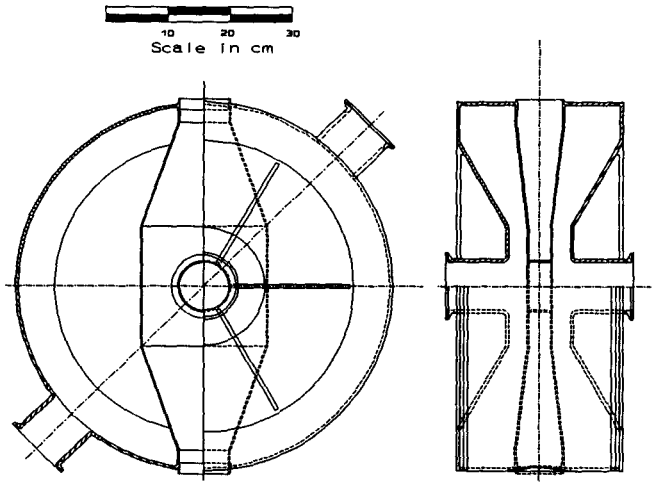

Figure 2. 175 MHz, β=0.125, 2-gap spoke resonator.

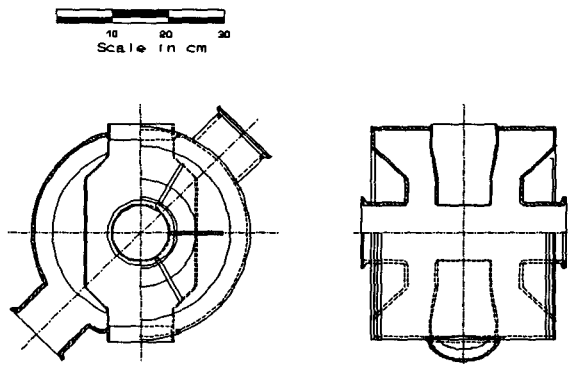

Figure 3. 350 MHz, β=0.45, 2-gap spoke resonator.

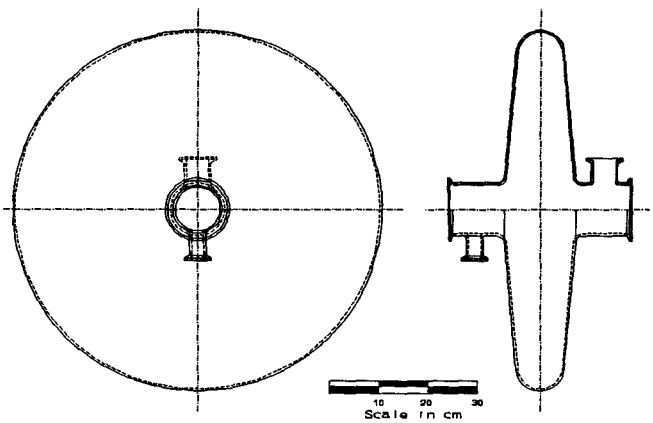

Figure 4. 350 MHz, β=0.45, single-cell TM_{010} resonator.

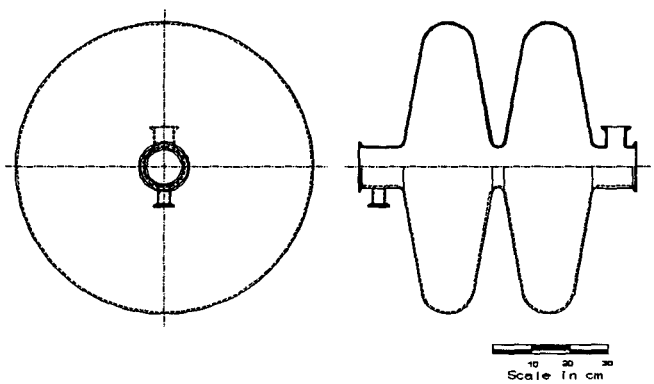

Figure 5. 350 MHz, β= 0.8, 2-cell TM_{010} resonator.

Table 2. Comparison of resonator properties.

	#1	#2	#3	#4
B_p/E_{acc}[G/(MV/m)]	122	125	41.6	35.9
R_{sh}* (10^5 MΩ)	1.3	1.5	1.2	6.7
R_{sh}/Q (Ω)	47.1	121	51.3	205
P (W)*†	2.73	9.65	9.0	14.5
ΔV (MV)†	0.6	1.2	1.0	3.1
Diameter (cm)	60	38	74	76

*Assumes BCS R_s at T = 4.2 K, †At E_{acc} = 6 MV/m.

It remains to be determined where to transition from the spoke geometry to multicell structures in a full linac design. It is also of interest to determine the optimum number of gaps or cells for each structure. Beam dynamics and the availability of rf power influence this question. The required lattice period of focusing elements will be shorter at lower velocities. A requirement that the linac be operable when one or more structures have failed will place an additional constraint on structure length. The amount of rf power which may be input to the cavity will be limited by the capability of the coupler, and this places the most stringent restriction on structure length in high-current linacs.

3. Superconducting RFQs[5,9,10]

Superconducting structures are characterized by high intrinsic Q and correspondingly narrow bandwidth. For low-current applications where beam loading will be negligible, superconducting structures can be sensitive to frequency variations caused by external noise and microphonics, and ponderomotive instabilities. This problem was solved for low-velocity structures by a combination of electronic control and the development of mechanically stable geometries. Thus, mechanical rigidity is a principal consideration in the design of low-current SCRFQs.

The manufacturing techniques used for superconducting structures are different than those used for normal-conducting structures and will have an impact on the electromagnetic and mechanical design. For example, the only joining method in high-current regions is electron-beam welding. Demountable joints are avoided or used only in low magnetic field regions, and sliding contacts have not been successfully developed for superconducting structures. Thus, the amount of adjustment that can be accomplished on a completed SCRFQ will probably be limited to mechanical deformation. Adjustments by sliding contacts and shimming which have been used extensively in normal-conducting RFQs will probably not be useful for SCRFQs. Thus the designs of SCRFQs will have to be robust, in the sense that the electromagnetic mode purity will need to be insensitive to dimensional inaccuracies.

Preliminary designs of high-current superconducting ion accelerators indicate that the transition between the RFQ and the "drift tube" cavities will take place at higher energy than in normal conducting accelerators, typically around 5 MeV/amu. Even taking into account the possibility of higher gradient, this indicates that the capability of building long SCRFQs might be beneficial. Since, for a given amount of mode mixing, the required manufacturing tolerances decrease as the square of the length,[11] it is even more important to develop designs for high-current SCRFQs which are relatively insensitive to manufacturing inaccuracies.

The third important consideration in the design of SCRFQs is the necessity of cooling to remove the heat generated by the rf currents. Furthermore, for high-current RFQs, there will always be a certain amount of beam impingement, and additional cooling will be required to remove the heat deposited. Thus, the challenge for SCRFQs is to develop designs which are rigid, simple to manufacture, provide a quadrupole mode isolated from other modes, and are easily cooled.

Two main designs of RFQs have evolved in the last decade (see, for example, Ref 11-12). The first one, the 4-vane RFQ geometry, is basically a waveguide modified to emphasize the quadrupole TE_{21} mode. This geometry leads to designs which are conceptually simple, with a high degree of symmetry, and mechanically rigid. Its main drawback is that the dipole TE_{11} mode is often close to the quadrupole mode, and small perturbations of the quadrupole symmetry lead to strong mixing between the quadrupole and the dipole modes. The near degeneracy results from the fact that the fields in the four quadrants overlap only in a small region, near the beam line. Ways of removing the degeneracy by increasing the frequency of the dipole mode have been found such as strapping opposite vanes together by vane coupling rings.[13] Such a solution, however, would be difficult to reconcile with the manufacturing techniques of

niobium resonators.

The other often-used design is the 4-rod structure. This structure relies more on a 'lumped element' design than the distributed design of the 4-vane geometry. Its main advantage is that the quadrupole mode is widely separated from other modes, resulting in a robust design. However, it is less attractive for SCRFQs, because it may be less mechanically rigid and more difficult to build and cool than a '4-vane' geometry.

We have investigated designs which have the advantages of both the 4-vane and 4-rod designs and provide a continuous evolution between the two. This intermediate geometry seems well suited for SCRFQs and may also have advantages for normal-conducting RFQs.

In an ideal RFQ design, the quadrupole mode would have the lowest frequency and be widely separated from the dipole mode. In the typical 4-vane geometry, however, the quadrupole mode frequency is close to the dipole mode frequency and slightly higher. This near degeneracy can be understood in lumped-element representations of both modes of oscillations, which are identical, except for a small additional capacitance between opposite vanes for the dipole mode.[14] This results from the fact that there is no overlap of the magnetic field of adjacent quadrants. Since, in the dipole and quadrupole modes, magnetic fields in adjacent quadrants have opposite configuration, providing an overlap or coupling of the magnetic fields would remove the degeneracy and increase the frequency splitting.

We have pursued this idea by calculating with MAFIA[15] the frequencies of the dipole and quadrupole modes of an infinite waveguide of the 4-vane geometry with periodic cutouts through the vanes as shown in Fig. 6. These cutouts allow magnetic coupling between adjacent quadrants. The results of the numerical calculations are shown in Table 2. It can be shown by energetic arguments that, this way, the quadrupole mode frequency is lowered by an amount between one and two times the decrease of the dipole mode frequency. This conclusion is supported by Fig. 7 which summarizes all the results. Thus, with cutouts which are large enough, one obtains a geometry which is still simple, with a high degree of symmetry, but, at the same time, has a quadrupole mode which is lower and widely separated from the dipole. This geometry also offers a continuous evolution from the 4-vane to the 4-rod geometry. In the most extreme case of large cutouts, the structure consists of 4 rods periodically supported by posts located in a quadrupole pattern.

While MAFIA is very powerful in predicting various electromagnetic properties of the structure, it is quite time consuming to investigate their dependence on all the dimensional parameters, and it does not give much physical insight. In the case of cutouts extending to the outside diameter of the structure (b=0 in Fig. 6), a transmission-line model can be developed to calculate the electromagnetic properties of the quadrupole mode of the infinite waveguide. The wavelength λ associated with the resonant frequency of the quadrupole mode satisfies the equation

$$2\tan\frac{2\pi h}{\lambda}\left\{\tan\left[\frac{2\pi}{\lambda}\left[\frac{L-t}{2}\right]\right]+\frac{\pi t}{\lambda}\right\}=\frac{\epsilon}{C}\left[\frac{2t}{g}+\alpha\right],$$

where C, the capacitance per unit length of the rod, is given in pF/m by[16]

$$C=\frac{39.365}{\cosh^{-1}\left[\frac{d+r}{r\sqrt{2}}\right]}+\frac{31.045}{\frac{d}{r}+1-\sqrt{2}}+25.28\ln\left[1+\frac{f}{d+r}\right],$$

α is a constant which, for our dimensions, is of the order of 3, [17] and $g \simeq \frac{1}{2\sqrt{2}}(2R-h)-r$.

The right-hand side of the characteristic equation for λ is valid for $t < L - \frac{\alpha g}{2}$. When $L - \frac{\alpha g}{2} < t < L$, then the right hand side is replaced by $\frac{\epsilon}{C}\frac{2L}{g}$.

This transmission-line model has been used to calculate the quadrupole-mode frequency for the geometry shown in Fig. 6 with b=0 and h=8.1 cm, for a wide range of cutout size a and period L. In all the cases the calculated frequency was within a few percent of that obtained with MAFIA.

TABLE 2
Results of MAFIA calculations for various cutouts of the vanes

R = 12 cm, d = 1.0 cm, r = 1.0 cm

L (cm)	t (cm)	a (cm)	h (cm)	b (cm)	Quad. (MHz)	Dipole (MHz)	fd-fq (MHz)
25	25	0	-	-	292.4	282.2	-10.2
25	21	4	2.7	0	291.2	281.2	-10.0
25	21	4	5.4	2.7	291.2	281.2	-10.0
25	21	4	8.1	5.4	291.6	281.5	-10.1
25	21	4	5.4	0	290.2	280.4	- 9.8
25	21	4	8.1	2.7	290.7	280.8	- 9.9
25	21	4	8.1	0	289.7	280.0	- 9.7
25	13	12	2.7	0	273.8	271.0	- 2.8
25	13	12	5.4	2.7	272.6	270.4	- 2.2
25	13	12	8.1	5.4	276.4	272.5	- 3.9
25	13	12	5.4	0	263.5	263.9	0.4
25	13	12	8.1	2.7	258.7	260.0	1.3
25	5	20	2.7	0	232.5	244.8	12.3
25	5	20	5.4	2.7	229.5	242.0	12.5
25	5	20	8.1	5.4	237.7	247.0	9.3
25	5	20	5.4	0	211.0	227.3	16.3
25	5	20	8.1	2.7	214.5	228.7	14.2
25	5	20	8.1	0	202.1	218.1	16.0
20	5	15	8.1	0	225.1	236.8	11.7
30	5	25	8.1	0	183.8	201.2	17.4

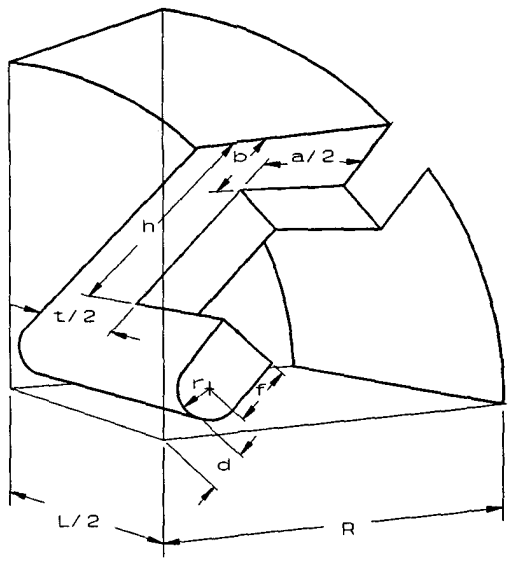

Figure 6 Schematic drawing of one quadrant of the periodic quadrupole waveguide. The full geometry can be obtained by a reflection around an end face and has a periodicity L.

This transmission-line model can also be used to calculate other electromagnetic properties, such as the z-dependence of the voltage on the tip of the vane, the energy content, currents, shunt impedance, etc.

We have also addressed some beam-dynamics and design issues associated with the development of high-current superconducting RFQs. In the beam current range of 25 mA to 100 mA, thermal-management considerations suggest that a tolerable level of beam impingement in a superconducting RFQ is 0.5% or less. Designing a structure with better than 99% transmission presents special challenges. For one, no present beam-dynamics code achieves the required accuracy. Another problem is that the design procedures suitable for conventional RFQs, which use a hard-wired prescription based on Kilpatrick factor, field enhancement coefficient, and constant capacitance of the rf structure, may be neither optimal nor desirable for SCRFQs.

As a general guideline, SCRFQs must have a fairly large aperture equal to at least 5 times the

rms beam radius. To accommodate the demand for strong transverse focusing, one should choose a low frequency since superconducting resonators do not seem to suffer from the frequency-dependent electric-field breakdown.

Longitudinal transmission is affected by the RFQ bunching rate. The trade-off is between the increased particle capture and the overall length of the accelerator. By increasing the energy at the end of the gentle buncher, thereby causing the beam to be bunched at a lower pace as it is accelerated, we can achieve design transmissions above 99%. The overall length of the RFQ would typically rise quadratically with the energy increase.

For example, we analyzed in detail a 25 mA, 200MHz RFQ and we found that raising the beam transmission from 97.7% to 99.6% to 99.9% would mean respective length increases from 2.7m to 4.3m to 6.0m. We have also looked at the frequency choice for SCRFQs. In general, lower frequency is preferable for better transmission characteristics. However, as a rule, lower frequency leads to a larger emittance growth.

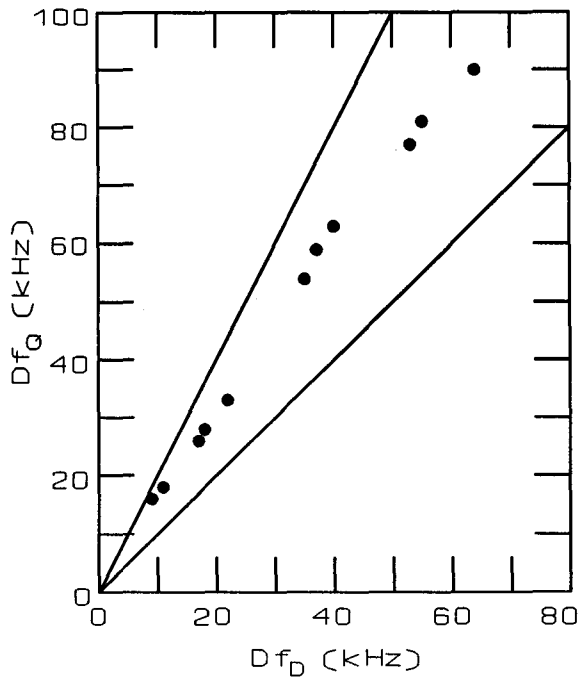

Figure 7, Decrease of the quadrupole mode frequency vs. decrease of the dipole mode frequency for the geometry of Fig. 6 and the various cutouts shown in Table 2.

IV. BEAM PHYSICS

1. Emittance Growth and Halo Formation

We recently introduced a semianalytic formalism describing the dynamics of transverse emittance growth and halo formation in nonrelativistic, mismatched beams arising as a consequence of nonlinear space-charge forces.[18-20] The formalism is based on a two-component model of the time-dependent distribution function of particles in the phase-space of a single particle. The Fokker-Planck equation governs the evolution of the coarse-grained component of the distribution function. It incorporates coefficients of dynamical friction and diffusion in velocity space which result from the fine-grained component of the distribution function. Turbulence excited as a consequence of charge redistribution enhances these coefficients and converts free energy due to mismatch into thermal energy. Dynamical friction and diffusion generate emittance growth and halo by injecting particles into high-amplitude orbits. They also dissipate any fine structure present in the beam at injection. Heating and relaxation of space-charge-dominated beams can occur during beam transport, as observed in laboratory experiments and numerical simulations.[21] This is a serious concern for high-current cw linacs in which halo-induced radioactivation of the accelerator walls must be suppressed to enable safe hands-on maintenance.

In a turbulent beam, the simultaneous interactions of a particle with many rather distant particles dominate binary coulomb interactions with nearby particles. This circumstance generates dynamical friction and diffusion in velocity space, and the spectrum of electric-field fluctuations determines the friction and diffusion coefficients.[22] We do not know these coefficients a priori; however, it should be

possible to infer them by studying individual particle orbits in N-body simulations.[23] In general, the coefficients may be expected to be functions of position, velocity, and time. In our formulation of the problem, we ignore the position and velocity dependencies and model the beam as a fluctuating fluid in which constituent particles execute Brownian motion. The diffusion coefficient is expressed as $D=ßkT/m$, in which ß is the relaxation rate, k is Boltzmann's constant, m is the single-particle mass, and T is the "diffusive temperature". We adopt a physically plausible phenomenological model of the time dependence of the diffusion coefficient by letting $T = T_\infty + (T_0-T_\infty)\exp(-ß_s t)$. Starting from temperature T_0, the beam strives to reach a Maxwell-Boltzmann distribution with temperature T_∞, and the heating occurs at the rate $ß_s \geq ß$ associated with "strong" turbulence. The ratio T_∞/T_0 is calculated from the available free energy.[24]

In summary, the physical picture of the microscopic dynamics is as follows. The mismatched beam becomes turbulent as a consequence of charge redistribution soon after injection into the accelerator, or passing through a transition in the accelerator.[21] If the beam is strongly mismatched in shape and size, the associated free energy will be large, and the beam will be strongly turbulent; otherwise, the beam will be weakly turbulent. After much of the free energy is converted into heat, electric-field fluctuations associated with residual weak turbulence and with beam oscillations further relax the beam. Once the beam has executed several plasma oscillations, it reaches a mixed quasi-steady state described by a distribution function which contains a coarse-grained part resembling Maxwell-Boltzmann and a fine-grained part consisting of diminishing localized field fluctuations. Of course, were the accelerator infinitely long, binary Coulomb collisions would eventually drive the beam to strict Maxwell-Boltzmann equilibrium. The difficult problem of refining and quantifying our oversimplified Fokker-Planck coefficients from first principles by studying individual particle orbits remains.

To solve the coupled Fokker-Planck and Poisson equations self-consistently, we decompose the coarse-grained distribution function into complete sets of orthogonal polynomials in coordinates and velocity components. This has been done for one-dimensional sheet beams[19] and fully two-dimensional beams.[20] The decomposition results in an infinite set of first-order, nonlinear differential equations for the time-dependent expansion coefficients which is fully equivalent to the Fokker-Planck-Poisson equations. Upon solving this set of equations, we have a self-consistent expression for the distribution function from which we may calculate any desired moment as a function of time, including the particle-density profile, the rms beam size, and the emittance.

We have written a FORTRAN code for implementation on PCs to solve for the expansion coefficients associated with a cylindrically symmetric beam. The code has been benchmarked against a closed-form, analytic solution of the Fokker-Planck equation in which the orbits are all harmonic oscillators. It has also been verified to provide the correct final distribution function corresponding to thermodynamic equilibrium and for which the density profile can be calculated numerically directly from Poisson's equation. The solution process involves truncating the series of equations, solving the truncated series, then increasing the number of equations and solving the bigger series. If the solutions substantially agree, then one knows that a sufficient number of terms has been retained in the truncation.

We provide here an example which we derived for direct comparison with the analytic solution based on harmonic-oscillator models of the orbits to highlight the effects of the non-linear space-charge forces. We consider a continuous, linear focusing channel with angular betatron frequency ω into which a beam with a Gaussian particle-density profile and Maxwellian velocity distribution is injected. The rms radius of the Gaussian beam is 1.2, where the unit of length is $(2kT_0/m\omega^2)^{1/2}$. The rms radius of the equilibrium (matched) beam is 1.458. This example therefore resembles a transition to weaker focusing. The ratio of the average Debye length[25] of the matched beam to its rms radius is 0.471, which indicates explicitly that space-charge forces are important to the beam dynamics, and therefore the beam is also

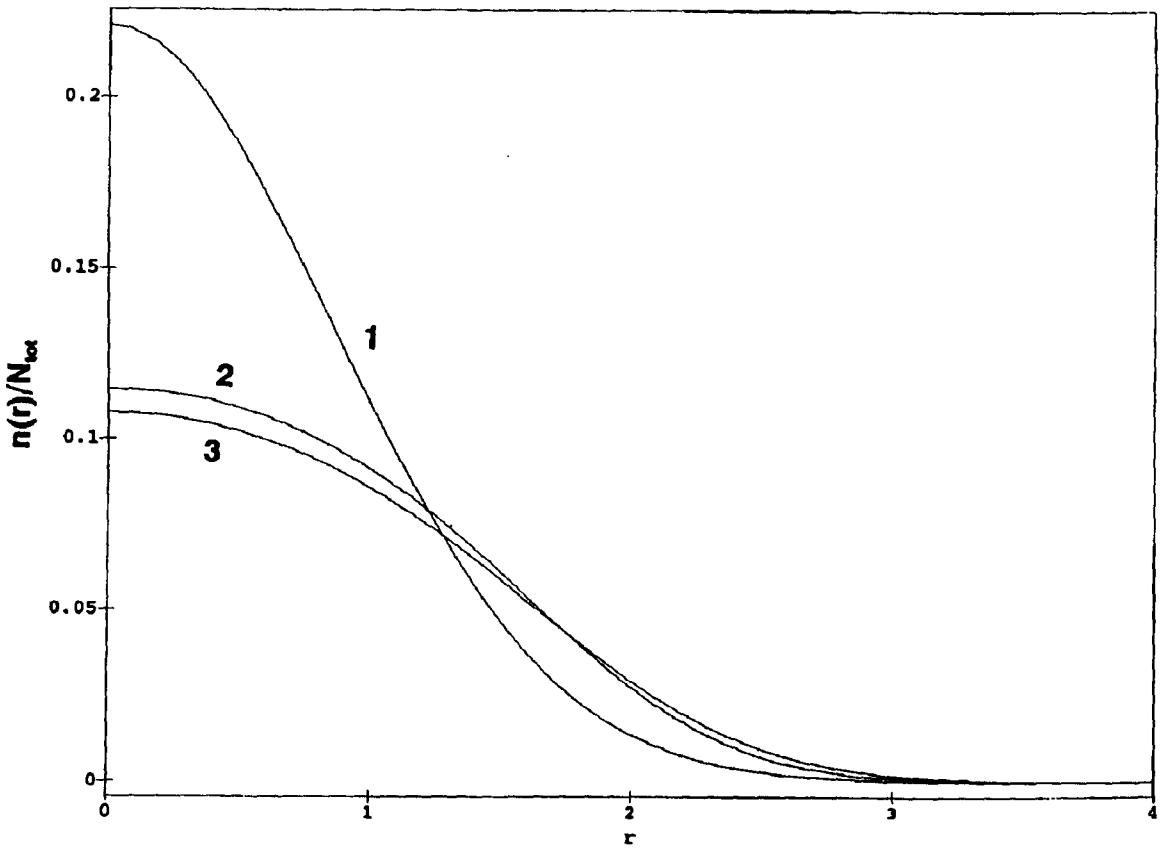

Figure 8. Particle-density profiles for example in text: rms-mismatched input beam (1); equilibrium beam with no heating (2); equilibrium beam with heating (3).

mismatched in shape. The ratio of final-to-initial temperature is calculated from the mismatch[24] to be $T_\infty/T_0 = 1.211$. The particle-density profiles of the initial beam, the matched beam, and the final beam are shown in Fig. 8. The input beam is modestly (20%) mismatched, and it is believed that existing techniques for accelerator design would keep mismatches at transitions to within this level.[26] In view of this modest mismatch, we assume the turbulence is always weak and take $ß_* = ß$. Furthermore, we assume for this example that $ß = 0.05\omega$.

Evolution of the rms radius and rms emittance normalized to their initial values are shown in Fig. 9. For comparison, curves calculated analytically assuming all the orbits are harmonic oscillators are also shown. It is clear that, on average, one dynamical effect of the nonlinear space-charge forces is to throw the particles farther away from the beam axis than the linear-force theory would predict, as one would intuitively expect.

Evolution of the "halo" is illustrated in Fig. 10. This figure shows the number of particles lying outside fixed radii equal to 1, 1.5, and 2. Curves calculated analytically assuming all the orbits are harmonic oscillators are also shown, and once again it is seen that the nonlinear space-charge forces tend to throw particles farther away from the beam axis. It is also seen that, in this example, and for these fixed radii, the halo is somewhat more prominent in the earlier stages of evolution than in the later stages.

In summary, we have developed a formalism for calculating emittance growth and halo formation in high-current beams for which space charge is important. The formalism is helpful in that, compared

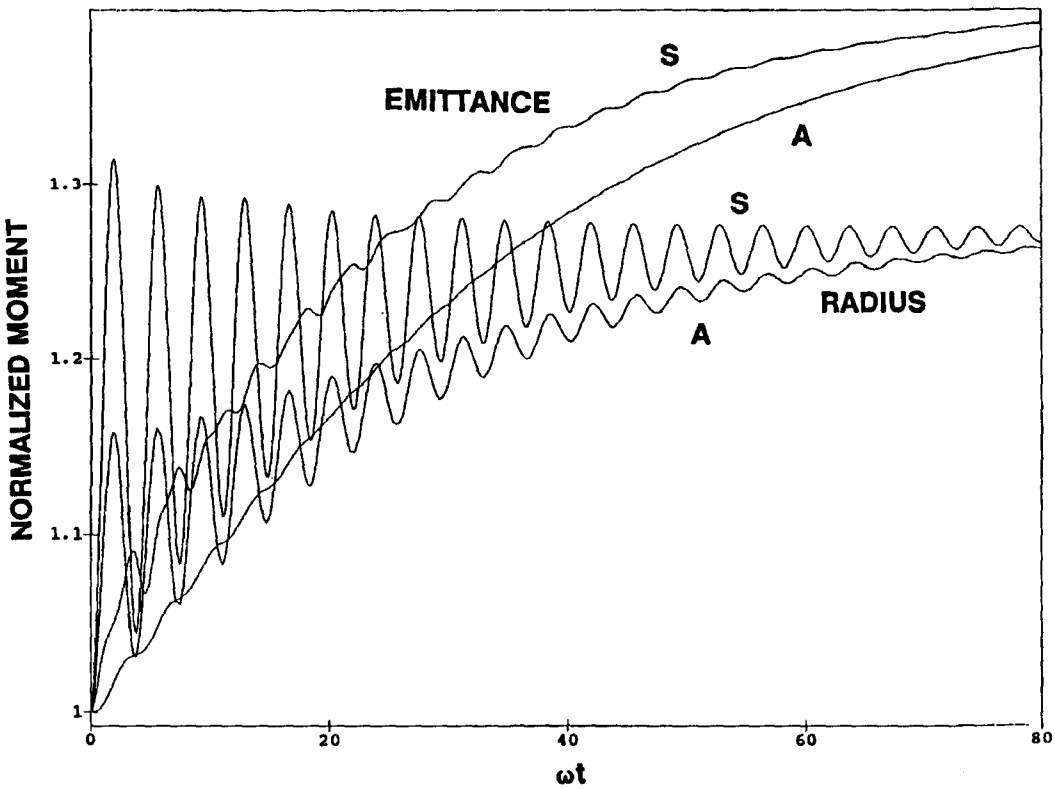

Figure 9. Rms radius, emittance normalized to t=0. Self-consistent solutions are denoted "S". Analytic solutions with harmonic-oscillator orbits are denoted "A".

to N-body simulations, it leads to fast computation of the transient dynamics. However, it incorporates an oversimplified model of the very complicated microscopic dynamics which involves at least one free parameter representing the relaxation rate, and which therefore limits its predictive capability. Accordingly, future work should focus on improving this model with the ultimate goal of including a self-consistent calculation of the Fokker-Planck coefficients.

2. *Cumulative Beam Breakup*

We developed a new analytic formalism of cumulative beam breakup (BBU) which is applicable to both low-velocity ion and high-energy electron linacs.[27] The formalism is based on Fourier analysis of the equation of transverse motion.

Steady-state BBU, which is of principal concern in cw linacs, was characterized in terms of the accelerator and beam parameters, the ratio of deflecting-mode and bunch frequencies, the bunch length, and the charge distribution within each bunch. The latter two parameters are of special importance in low-velocity beams. For a beam of point bunches, steady-state BBU is nearly independent of the effective Q of the wake fields except near the zero crossings of the wake function where the deflecting-mode frequency is an even-integer multiple of the bunch frequency. Strongly peaked resonances occur in these regions which can be suppressed by lowering the effective Q of the wake fields, and they are generally less pronounced with bunches of finite length, the exception corresponding to extremely short, but still finite, bunches. The deflecting fields tend to distort bunches of finite length, leading to emittance growth and degraded beam quality. Unbunched particles comprising a diffuse longitudinal halo between the bunches respond to the deflecting fields but do not excite them. These particles can be deflected more

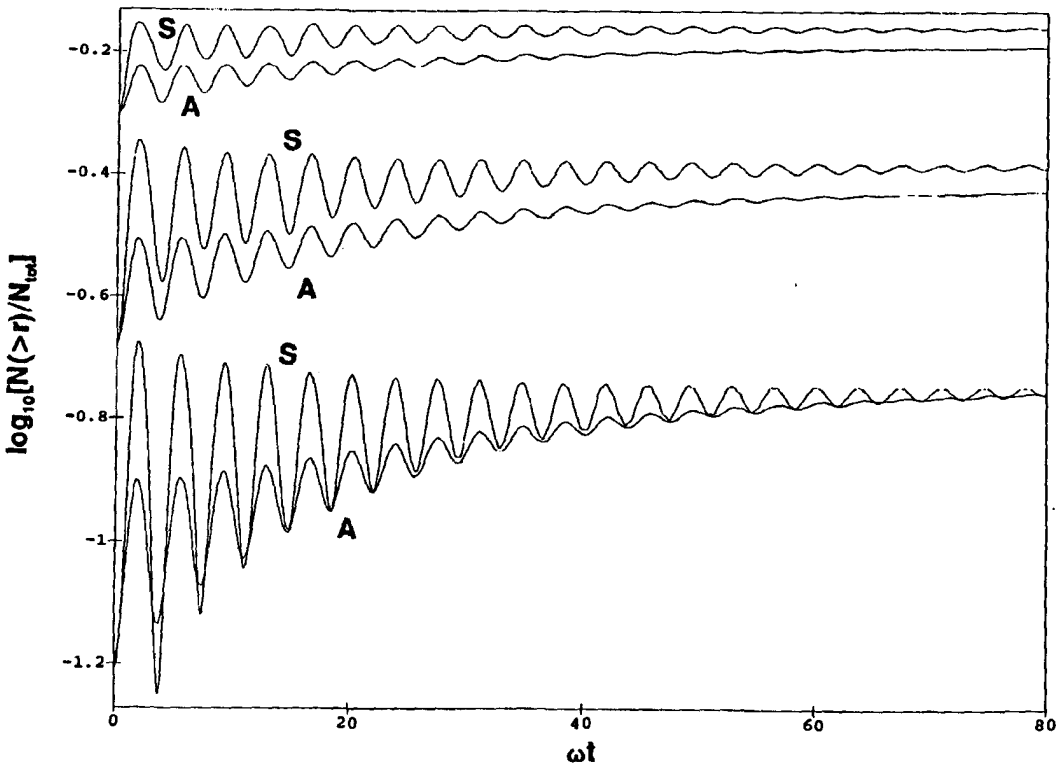

Figure 10. Fractional number of particles outside r=1 (top), r=1.5 (center), and r=2 (bottom). "S": self-consistent solutions; "A": analytic solutions.

than the bunches themselves. If allowed to impinge on the accelerating structures, they will contribute to activation over the long-term operation of the linac. Bunch distortion and halo displacement are both accentuated near the resonances. Steady-state BBU can also be considerable in the presence of random initial conditions of the bunches at the linac entrance. For example, with a beam of point bunches, a resonance occurs if a harmonic of the characteristic frequency of the correlation function for the bunch displacement at the linac entrance is close to the characteristic frequency of the wake function, and strong deflecting fields may then be generated. Sufficiently strong transverse focusing will suppress all of these potential problems associated with steady-state BBU.

A distribution of deflecting-mode frequencies in the constituent cavities of a linac can lead to Q-independent damping of both transient and steady-state cumulative BBU. We extended the BBU formalism to investigate this circumstance by replacing the single-mode wake function with an effective wake function which depends strongly on the probability density of the deflecting-mode frequencies.[28] This replacement is valid provided the transverse displacement does not change significantly over distances comparable to the correlation length of the deflecting-mode frequencies.

The rate of approach to the steady state depends strongly on the shape of the probability density. For example, the results for long pulses in the limits of weak and strong focusing indicate that a Gaussian probability density of the deflecting-mode frequencies distributed around the mean angular frequency ω_0 generates a faster decay to the steady state than does a Lorentzian probability density. Specifically, during decay with weak focusing and infinite Q the envelope decays like $\exp(\Gamma\omega_0 t)$, where $\Gamma\omega_0 t \propto -(\omega_0 t)^{5/3}$ for the Gaussian and $\Gamma\omega_0 t \propto -\omega_0 t$ for the Lorentzian, and with strong focusing the exponent behaves like $\Gamma\omega_0 t \propto -(\omega_0 t)^{3/2}$ for the Gaussian and again like $\Gamma\omega_0 t \propto -\omega_0 t$ for the Lorentzian. This is caused by the faster decay of the effective wake function associated with the Gaussian.

3. Alternating-Phase Focusing

We have developed a new model of alternating-phase focusing (APF) dynamics applicable to ion linacs with short, independently controlled superconducting cavities. Previous works in the literature[29-33] address APF primarily in the context of a discrete number of accelerating gaps spaced in a predetermined manner to achieve particular values of synchronous phase in each gap (as is the case in the Wideroe linac or the Alvarez DTL). By contrast, low-ß cavities of the type described in Section III present a more flexible approach to APF: the cavities are short, can be independently controlled in adjusting both the phase and the amplitude of the electric field, and were shown to produce very high accelerating gradients.[4,6] Essential APF physics for a linac using such cavities is derived from the equations of motion in a cylindrically symmetric traveling wave with continuous periodic phase and amplitude modulation.

In our model, we choose the modulation to be sinusoidal and, to first order, neglect effects of a velocity change in one APF period. The model gives analytical predictions of the linear stability region and the overall longitudinal acceptance in terms of a few universal parameters: equilibrium synchronous phase, phase modulation amplitude, length of APF period, and incremental energy gain, as well as the strength and the relative phase of the amplitude modulation. Using standard mathematical techniques for periodic systems, we have derived formulae for the longitudinal acceptance accurate to the second order in the deviation from the synchronous phase, $\Delta\phi$. Computer simulations indicate that for most practical cases the second-order approximation gives an error of no more than 10% in the acceptance computation. Numerical calculations show that the maximum separatrix width achievable in the low-β zero-current proton linacs with APF is about 45° in $\Delta\phi$. The model predicts that radial stability does not appear to be an issue. As suggested in the early work on APF,[29] the longitudinal acceptance region can be increased by simultaneous modulation of the accelerating amplitude. For the first time, our model quantifies the effects of the amplitude modulation. We have derived modified equations of motion and solved for the second-order acceptance in the case of the amplitude and the synchronous phase being modulated with the same frequency. The model is thought to be a good tool for analyzing the applicability of APF in various regimes of superconducting ion accelerators. It captures all the essential aspects of the APF physics and lends itself to analytical solutions.

V. CONCLUSIONS

Radiofrequency superconductivity offers a number of advantages for high-current, high-duty-factor linacs, among these is the ability to open up the cavity apertures to mitigate beam impingement and its associated radioactivation. The cavities also may be expected to operate at a higher real-estate gradient than their normal-conducting counterparts. There are no known show-stoppers for rf superconductivity in these applications; the associated beam physics is beginning to be understood, and appropriate accelerating structures have been designed.

An important uncertainty in the design of these linacs is the projected capability of rf power couplers. Coupler development and continued beam-physics research are key components of the development path. A more important and fundamental component, however, is a high-current ion-beam test of superconducting structures.[6]

VI. ACKNOWLEDGEMENTS

This work was supported by the U.S. Department of Energy under contract W-31-109-ENG-38 and by the Strategic Defense Initiative Organization.

VII. REFERENCES

1. M. Barbier, Induced Radioactivity, North Holland (1969).
2. D.H. Perkins, Introduction to High-Energy Physics, (Addison-Wesley, Reading, MA, 1972), p. 29.
3. N.I. Golubeva, A.S. Pashnekov, Yu.V. Senichev, and E.N. Shaposhnikova, "Problems of Beam Loss in Intense Ion Linear Accelerators", *Proceedings of the 1988 Linear Accelerator Conference*, 669 (1988).
4. J.R. Delayen, C.L. Bohn, and C.T. Roche, "Niobium Resonator Development for High-Brightness Ion Beam Acceleration", *IEEE Trans. Magnetics*, **MAG-27**, 1924 (1991).
5. J.R. Delayen, C.L. Bohn, W.L. Kennedy, L.Sagalovsky, "Design Considerations for High-Current Superconducting RFQ", *Proc. 1993 Particle Accelerator Conference*, Washington, DC, 17-20 May 1993 (in press).
6. J.R. Delayen, C.L. Bohn, W.L. Kennedy, G.L. Nicholls, C.T. Roche, and L. Sagalovsky, "Recent Developments in the Application of RF Superconductivity to High-Brightness and High-Gradient Ion Beam Accelerators", *Proceedings of the 5th Workshop on RF Superconductivity*, **DESY Report No. M-92-01**, 376 (1992).
7. J.R. Delayen, W.L. Kennedy, and C.T. Roche, "Design and Test of a Superconducting Structure for High-Velocity Ions", *Proceedings of the 1992 Linear Accelerator Conference*, **AECL Report No. 10728**, pp. 695-697 (1992).
8. T.P. Wangler, "High-Brightness Injectors for Hadron Colliders", in Frontiers of Particle Beams: Intensity Limitations, (Springer-Verlag, Berlin, 1992), pp. 542-561.
9. A. Schempp, H. Deitinghoff, J.R. Delayen and K.W. Shepard, "Design and Application Possibilities of Superconducting Radio-Frequency Quadrupoles", *Proceedings of the 1990 Linear Accelerator Conference*, Los Alamos Publication **LA-12004-C**, 79 (1991).
10. J.R. Delayen and W.L. Kennedy, "Design and Modeling of Superconducting RFQ Structures", *Proceedings of the 1992 Linear Accelerator Conference*, **AECL Report No. 10728**, pp. 692-694 (1992).
11. J.W. Staples, "RFQs - An Introduction", in *The Physics of Particle Accelerators*, AIP Conference Proceedings **249**, 1483 (1992).
12. A. Schempp, "Recent Progress in RFQs", *Proceedings of the 1988 Linear Accelerator Conference*, **CEBAF-Report-89-001**, 460 (1989).
13. H.R. Schneider, H. Lancaster, "Improved Field Stability in RFQ Structures with Vane Coupling Rings", IEEE Trans Nucl. Sci. **NS-30**, 3007 (1983).
14. M. Weiss, "Radio-Frequency Quadrupole", in *Proceedings Second General Accelerator Physics Course, CERN Accelerator School*, **CERN 87-10**, 196 (1987).
15. *MAFIA User Guide*, the MAFIA Collaboration, DESY, LANL, and KFA (1988).
16. I. Ben-Zvi, A. Jain, H. Wang, A. Lombardi, "Electrical Characteristics of a Short RFQ Resonator", *Proceedings of the 1990 Linear Accelerator Conference*, Los Alamos Publication **LA-12004-C**, 73 (1991).
17. R.E. Collins, *Field Theory of Guided Waves*, IEEE Press, 2nd edition, p. 282 (1991).
18. C.L. Bohn, "Transverse Phase-Space Evolution in Non-Stationary Charged Particle Beams", *Proceedings of the 1992 Linear Accelerator Conference*, **AECL Report No. 10728**, pp. 471-473

(1992).
19. C.L. Bohn, "Transverse Phase-Space Dynamics of Mismatched Charged-Particle Beams", *Phys. Rev. Lett.*, **70**, 932 (1993).
20. C.L. Bohn and J.R. Delayen, "Halo Formation in Mismatched, Space-Charge-Dominated Beams", *Proceedings of the 1993 Particle Accelerator Conference,* Washington, DC, 17-20 May 1993 (in press).
21. D. Kehne, M. Reiser, H. Rudd, "Experimental Studies of Emittance Growth in a Nonuniform, Mismatched, and Misaligned Space-Charge Dominated Beam in a Solenoid Channel", in *High-Brightness Beams for Advanced Accelerator Applications*, ed. W.W. Destler and S.K. Guharay, **AIP Conf. Proc. 253**, (AIP, NY, 1992), pp. 47-56; T.P. Wangler, "Emittance Growth from Space-Charge Forces", *ibid.*, pp. 21-40; R.A. Jameson, "Beam Halo from Collective Core/Single-Particle Interactions", **LANL Report No. LA-UR-93-1209**, March 1993.
22. S. Ichimaru, *Statistical Plasma Physics*, (Addison-Wesley, Redwood City, CA, 1992).
23. J.M. Dawson, "Particle Simulation of Plasmas", *Rev. Mod. Phys.*, **55**, 403 (1983).
24. M. Reiser, "Free Energy and Emittance Growth in Nonstationary Charged Particle Beams", *J. Appl. Phys.*, **70**, 1919 (1991).
25. M. Reiser and N. Brown, "Thermal Distribution of Relativistic Particle Beams with Space Charge", *Phys. Rev. Lett.*, **71**, 2911 (1993).
26. R.A. Jameson, private communication (1993).
27. C.L. Bohn and J.R. Delayen, "Cumulative Beam Breakup in Linear Accelerators with Periodic Beam Current", *Phys. Rev. A*, **45**, 5964 (1992).
28. C.L. Bohn and J.R. Delayen, "Influence of a Distribution of Deflecting-Mode Frequencies on the Transient Dynamics of Cumulative Beam Breakup", *Proceedings of the 1992 Linear Accelerator Conference*, **AECL Report No. 10728**, pp. 474-476 (1992).
29. V.V. Kushin, "On Increasing the Efficiency of Alternating-Phase Focusing in Linear Accelerators", *Atomnaya Energiya*, **29** (3) (1970); V.V. Kushin and V.M. Mokhov, "Amplitude Modulation of the Accelerating Field in a Linear Accelerator with Asymmetric Variable-Phase Focusing", *Atomnaya Energiya*, **35** (3) (1973).
30. A.S. Beley et al., "Some Properties of Longitudinal Motion in a 3-MeV Proton Accelerator with Variable Phase Focusing", *Zh. Tekh. Fiz.*, **51**, 656 (1981).
31. V.K. Baev and S.A. Minaev, "Efficiency of Ion Focusing by the Field of a Travelling Wave in a Linear Accelerator", *Zh. Tekh. Fiz.*, **51**, 2310 (1981); V.K. Baev, N.M. Gavrilov, S.A. Minaev and A.V. Shal'nov, "Linear Resonance Ion Accelerators with a Focusing Axisymmetric Accelerating Field", *Zh. Tekh. Fiz.*, **53**, 1287 (1983).
32. F.G. Garashchenko et al., "Optimal Regimes of Heavy-Ion Acceleration in a Linear Accelerator with Axisymmetric Variable-Phase Focusing", *Zh. Tekh. Fiz.*, **52**, 460 (1982).
33. H. Okamoto, "Beam Dynamics of Alternating Phase Focused Linacs", *Nucl. Instrum. Methods*, **A284**, 233-247 (1989).